Inorganic Chemistry

Article

pubs.acs.org/IC

Quest for Lead Free Relaxors in $YIn_{1-x}Fe_xO_3$ ($0.0 \leq x \leq 1.0$) System: Role of Synthesis and Structure

Rakesh Shukla,[†] Farheen N. Sayed,[†] Vinita Grover,*[,†] Sudhanshu K. Deshpande,[‡] Apurav Guleria,[§] and Avesh K. Tyagi*[,†]

[†]Chemistry Division, [‡]UGC-DAE Consortium for Scientific Research, and [§]Radiation and Photochemistry Division, Bhabha Atomic Research Centre, Mumbai 400085, India

ABSTRACT: The B-site tailored $YIn_{1-x}Fe_xO_3$ ($0.0 \leq x \leq 1.0$) series was synthesized by glycine-aided gel-combustion technique and subjected to extensive structural and electrical investigations. The temperature had tremendous bearing on the phase evolution exhibited by the system. The entire system crystallized as C-type metastable polymorph in the as−synthesized form. Hexagonal polymorphs of Fe^{3+}-rich compositions could be isolated by controlled heat treatment at 750 °C. Raman spectroscopic investigations showed that, while there is a general shrinkage of the lattice due to substitution of a smaller ion at In^{3+}-site, there is an apparent dilation of the Y−O bond, and this anomaly reflects in the electrical behavior exhibited by the system. The single-phasic hexagonal nominal compositions, $YIn_{1-x}Fe_xO_3$ ($0.0 \leq x \leq 0.3$), were also studied by impedance spectroscopy. The dielectric constant was found to drastically increase from 10 for $YInO_3$ to 1000 for $YIn_{0.7}Fe_{0.3}O_3$ at room temperature stressing the role of B-site tailoring on electrical behavior. More interestingly, careful substitution of Fe into $YInO_3$ could tune the electrical behavior from a dielectric to relaxor ferroelectric in the temperature range studied. The nominal composition $YIn_{0.7}Fe_{0.3}O_3$ showed a classical relaxor ferroelectric like behavior which is an important observation in context of the search for new lead free relaxor materials.

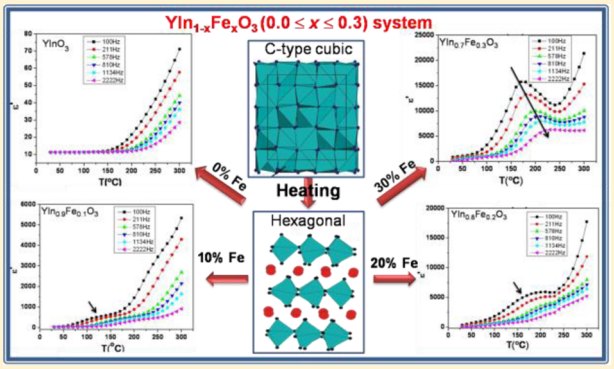

1. INTRODUCTION

The ABO_3-compounds have assumed center-stage in the research on composition−property relationships among oxides.[1−3] This can primarily be attributed to the flexibility or the range of the cations that can be substituted at A- and B-sites.[4] ABO_3 are generally associated with a cubic perovskite structure which is defined by a three-dimensional array of BO_6-octahedra wherein A occupies the 12-coordinated cuboctahedral site.[5] However, in most cases, there is a tilting of BO_6 octahedra in the case of a smaller A-ion to fill up the space, and the resulting structure is an orthorhombic perovskite. The kind of structure adopted by the ABO_3 class of compounds depends on the relative radii of A- and B- cations. It is in fact described by tolerance factor (t) given by $(r_A + r_O)/\sqrt{2}(r_B + r_O)$, which is also called the Goldschmidt tolerance factor for cubic and orthorhombic perovskites. It has been reported that for $t \leq 0.87$ ABO_3 crystallizes as a hexagonal structure (space group $P6_3cm$ and $P6_3/mmc$) which are basically different from the perovskite structure. These are layered structures, wherein A cation has the 7-fold coordination and the B cations are situated in the 5-fold trigonal bipyramidal sites. This hexagonal structure is only known for trivalent A cations, which may be smaller rare-earth ions (Gd−Lu, Sc), and in some cases In and the B cation can be Al, In, Ga, Mn, Fe, etc.[6−12]

Hexagonal ABO_3 have invoked considerable interest because of the existence of geometric ferroelectricity which is attributed to the physical arrangement of atoms in the lattice structure. The mechanism of ferroelectricity in these improper ferroelctrics is basically different from $BaTiO_3$- and $BiFeO_3$-based system.[13] These materials have been a front-area of research due to better probability of simultaneously obtaining magnetic and electrical ordering and discovering newer and better multiferroics. Very recently, they have also been shown as promising color pigment and catalysts.[14−16] A lot of research in this class of materials has been focused on $YMnO_3$.[17−20] Yttrium indate, $YInO_3$, belongs to the family of hexagonal rare-earth indates and has been investigated for interesting electrical behavior. It possesses a similar structure to $YMnO_3$ and is known to crystallize in space group $P6_3cm$ at ambient conditions. $YInO_3$ is known to exist in both paraelectric (space group $P6_3/mmc$) and ferroelectric forms (space group $P6_3cm$), and the transition between these two modifications is displacive in nature.[21] It is known that in these kinds of materials ferroelectricity is controlled by unequal Y−O bond lengths along the c axis and tilt of BO_5 trigonal bipyramids, which in turn are interrelated.[13,21]

Received: April 23, 2014
Published: September 10, 2014

dx.doi.org/10.1021/ic5009472 | Inorg. Chem. 2014, 53, 10101−10111

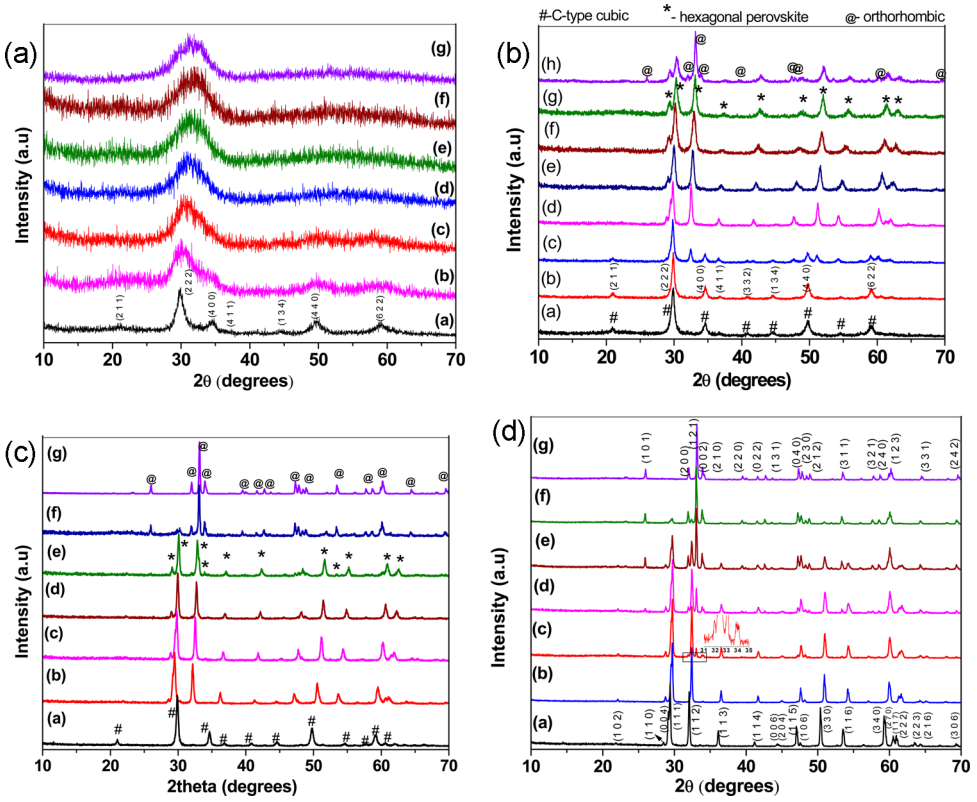

Figure 1. (a) Room temperature XRD patterns of $YIn_{1-x}Fe_xO_3$ compositions (a) $x = 0$, (b) 0.1, (c) 0.3, (d) 0.5, (e) 0.7, (f) 0.9, and (g) 1.0, prepared by gel-combustion method followed by calcination for 2 h at 600 °C. (b) Room temperature XRD patterns of $YIn_{1-x}Fe_xO_3$ compositions (a) $x = 0$, (b) 0.1, (c) 0.2, (d) 0.4, (e) 0.6, (f) 0.8, (g) 0.9, and (h) 1.0 after heat-treatment at 750 °C for 8 h. (#, C-type cubic; *, Hexagonal perovskite related structure; and @, orthorhombic perovskite). (c) Room temperature XRD patterns of $YIn_{1-x}Fe_xO_3$ compositions (a) $x = 0$, (b) 0.1, (c) 0.4, (d) 0.6, (e) 0.7, (f) 0.9, and (g) 1.0 after heat-treatment at 900 °C for 8 h. (#, C-type cubic; *, Hexagonal perovskite related structure; and @ , orthorhombic perovskite). (d) Room temperature XRD patterns of $YIn_{1-x}Fe_xO_3$ compositions (a) $x = 0$, (b) 0.4, (c) 0.5, (d) 0.6, (e) 0.8, (f) 0.9, and (g) 1.0 after heat-treatment at 1150 °C for 8 h; (Inset shows appearance of weak orthorhombic peaks in (c) $x = 0.5$ ($YIn_{0.5}Fe_{0.5}O_3$) composition in the $31 \leq 2\theta \leq 35$ range).

In addition to being novel electrical materials, rare-earth based hexagonal ABO_3-type oxides possess an additional advantage of being Pb-free materials. Most of the research activities on relaxor ferroelectric materials have focused on lead-containing systems such as PMN- and PZN-based solid solutions, (Pb,La)(Zr,Ti)O3 ceramics, etc., which is due to their larger material output coefficients. However, due to the well-known hazardous nature of lead,[22] there are increasingly growing restrictions on their prevalent use which infact necessitates the research on alternative Pb-free materials. Some common Pb-free relaxors being investigated consist of $BaTiO_3$–$BaSnO_3$ solid solutions.[23−26] However, in view of envisaged applications as multiferroic materials, these novel hexagonal ABO_3 compounds are superior since there is a greater possibility of achieving coupling between magnetic and electrical properties in these hexagonal materials as compared to perovskites. All these features make hexagonal rare-earth ABO_3 compounds a very lucrative class of materials worth investigating.

In our previous studies on rare-earth hexagonal indates, it was observed that hetero substitution on A- and B-site provides an important tool to tune the electrical behavior of these compounds.[27,28] It was observed that in the $GdIn_{1-x}Sc_xO_3$ ($(0.0 \leq x \leq 1.0)$ system, phase relation consisted of a very narrow hexagonal field and the relaxor behavior could be introduced in this hexagonal structure due to compositional disorder as a result of B-site substitution. In this direction, there is a curiosity to investigate whether a wider solubility of heteroatom at B-site retaining the hexagonal structure would lead to better electrical properties. However, this also implies that a judicious selection of the substituent cation, the one which is more amenable to trigonal bipyramidal co-ordination (unlike Sc^{3+}), needs to be done to increase the possibility of obtaining a wider hexagonal phase field.

In order to investigate this, $YInO_3$ (a known ferroelectric unlike $GdInO_3$ which was only postulated to be so[29]) was chosen as the host material and Fe^{3+} was substituted over the entire composition range. The present work explores the $YIn_{1-x}Fe_xO_3$ ($0.0 \leq x \leq 1.0$) system, its synthesis and extensive characterization by X-ray diffraction and Raman spectroscopic studies, and also the structural variations as a function of temperature. The work further explores the dielectric behavior of these nominal compositions by impedance spectroscopy to investigate the effect of B-site tailoring on electrical properties. An interesting structural−electrical behavior correlation could be established in this system.

2. EXPERIMENTAL SECTION

Y_2O_3, In_2O_3, $Fe(NO_3)_3{\cdot}6H_2O$, and glycine (AR grade) were used as the starting reagents. The gel combustion process was adopted for synthesis which is basically a redox reaction between an oxidant, usually metal nitrates, and a fuel like glycine, citric acid, etc.[30] The highlight of this preparative technique is that it provides a homogeneous atomistic level blending of the reactant ions in the

dx.doi.org/10.1021/ic5009472 | Inorg. Chem. 2014, 53, 10101−10111

solution which increases the probability of achieving single-phasic product after combustion in very short duration of time. In addition, the combustion method is a non-equilibrium process. In order to synthesize various nominal compositions in the $YIn_{1-x}Fe_xO_3$ ($0.0 \leq x \leq 1.0$) system, stoichiometric amounts of reactants were dissolved in a minimum amount of nitric acid. Glycine was used as fuel, and fuel-deficient conditions were employed for these syntheses. Due to low exothermicity of glycine-nitrate combustion in fuel-deficient proportions, nano powders with better powder properties are obtained with a possibility of isolating metastable modifications in some cases. For the synthesis of a representative nominal composition, $YIn_{0.5}Fe_{0.5}O_3$, typical amounts of reactants weighed were Y_2O_3 (5 mmol, wt = 1.1290 g), In_2O_3 (2.5 mmol, wt = 0.6941g), and $Fe(NO_3)_3.9H_2O$ (5 mmol, wt = 2.0200 g). These were dissolved in 20 mL of dil. HNO_3, and after the dissolution of these reactants, 8.3 mmol (wt = 0.6225 g) of glycine (50% fuel deficient condition) was added to this solution. The reactant solution was then slowly evaporated and made to undergo combustion after formation of highly viscous gel. The auto-ignition process resulted in voluminous powders which were calcined at 600 °C in static air for 2 h to remove any traces of carbonaceous residue. The obtained nanopowders were then heated at 750, 900, 1150, and 1250 °C in static air and slowly cooled (2 °C/min) to room temperature to study the phase evolution as the function of temperature.

X-ray diffraction (XRD) studies were performed using monochromatized Cu Kα radiation on a PANalytical Xpert Pro. Silicon was used as the external standard. The patterns were refined using Rietveld refinement, and lattice parameters were determined. Raman spectroscopic measurements were carried out on a micro/macro-Raman spectrometer (LABRAM-1, France) using a 488 nm line of an Ar^+ ion laser for excitation. The scattered Raman signal was collected using a single monochromator spectrometer equipped with a Peltier-cooled CCD detector in the backscattering geometry. Samples were used in the form of pellets, and the laser line was focused on a flat surface of the sample using an optical microscope (Olympus BX-40, 50x objective lens) connected to the spectrometer. The spectra recorded were averaged out of 50 scans with a time interval of 2 s and a resolution of 2 cm^{-1}.

The dielectric properties of the single phasic hexagonal $YIn_{1-x}Fe_xO_3$ (x = 0.0, 0.1, 0.2, and 0.3) compounds were measured over a temperature range from 30 to 300 °C (303−573 K) and over the frequency range of 100 Hz to 10 MHz using a Novocontrol Alpha-AN impedance analyzer (Novocontrol Technologies GmbH, Germany) equipped with a Quatro nitrogen gas cooling/heating system. Samples in the form of cylindrical pellets were sandwiched between two gold-plated electrodes in a parallel plate capacitor configuration. Samples were coated with silver paste for proper electrical contacts.

3. RESULTS AND DISCUSSION

3.1. X-ray Diffraction (XRD) Structural Studies. The $YIn_{1-x}Fe_xO_3$ ($0.0 \leq x \leq 1.0$) system was synthesized by self-assisted gel combustion method followed by calcination at 600 °C. In order to investigate the evolution of phase relations with temperature, all the nominal compositions synthesized in $YIn_{1-x}Fe_xO_3$ ($0.0 \leq x \leq 1.0$) system were heated at different temperatures. The XRD patterns of various nominal compositions as prepared (calcined), heated at 750 °C, 900 and 1150 °C are depicted in Figure 1a−d, respectively. The XRD patterns of the calcined powders revealed that all the nominal compositions show C-type structure, ($Ia\bar{3}$, Figure 1a). It must be noted that the actual synthesis temperature of these C-type solid solutions is not 600 °C. The *in situ* generated heat, during gel combustion, facilitates the formation of product. The reaction temperatures can be tuned by controlling the oxidant-to-fuel ratio in gel combustion, which facilitates the formation of solid solutions. Further, the diffusion path is much shorter due to atomistic blending of constituents in the gel, and hence lower temperatures are required for the reaction to take place. The external temperature of 600 °C was employed to calcine the powder obtained after gel combustion in order to remove any carbonaceous residue left in the product as the result of gel combustion.

Figure 1a reveals that there is a broadening of XRD peaks with increase in Fe^{3+} content. This implies that in addition to the nanosize of the crystallites the increase in fwhm can also be attributed to the strain induced in the lattice due to heteroatom incorporation. The systematic shift observed in the XRD peaks to higher angles confirms the solid solution formation in the entire homogeneity range. Further, this shift can be attributed to the decrease in the lattice parameter, on substitution of smaller ion Fe^{3+}(0.55 Å) for a larger ion In^{3+} (0.80 Å). The ionic radii reported by Shannon et al.[31] at co-ordination number, CN = 6, have been taken as the reference. Thus, the calcined powders of various nominal compositions show the single-phasic C-type phase relation throughout the whole composition ($0.0 \leq x \leq 1.0$) range of samples prepared at 600 °C (see Figure 5 for brevity).

The analysis of XRD patterns at 750 °C (Figure 1b) revealed an entirely different phase relation. It was observed that the nominal compositions, $YIn_{1-x}Fe_xO_3$ ($0.3 \leq x \leq 0.9$), have transformed from C-type to hexagonal phases. The nominal compositions with 20 mol % Fe^{3+} content is observed to be biphasic with both C-type and hexagonal phases. The C-type to hexagonal phase transition is a reconstructive phase transition, and thus, it is not unusual to observe a biphasic region in between two phases separated by a reconstructive phase transition. Pure $YInO_3$ and $YIn_{0.9}Fe_{0.1}O_3$, however, still exist as C-type polymorph. The other end member $YFeO_3$, though, is biphasic with hexagonal (majority) and traces of orthorhombic phases. The existence of Fe-rich compositions and $YFeO_3$ in hexagonal modifications is an unusual result, and its significance in terms of relative radii of cations and anions is discussed later in the manuscript. The lattice parameters were determined for the nominal compositions, ($YIn_{1-x}Fe_xO_3$ ($0.3 \leq x \leq 1.0$), existing as single-phasic hexagonal polymorph including that of x = 1.0 which is hexagonal-orthorhombic biphasic (see Figure 5) obtained after 750 °C heat treatment. These are depicted in Figure 2. There is decrease in the lattice parameter of the solid solutions with increase in Fe^{3+} -content. This, of course, can be attributed to the decrease in average B-site ionic radius on substituting In^{3+} with Fe^{3+}. Worth mentioning is the observation that decrease in c-lattice parameter is twice that

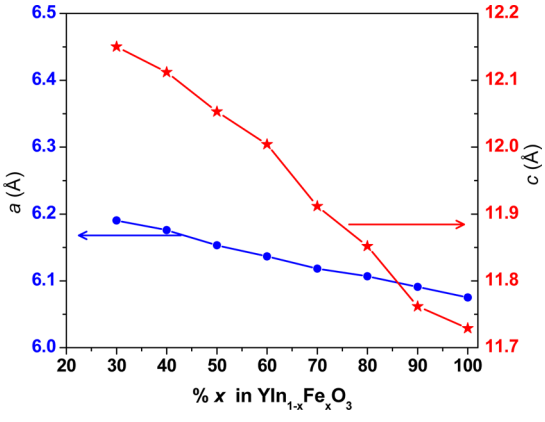

Figure 2. Lattice parameter variation in $YIn_{1-x}Fe_xO_3$ ($0.3 \leq x \leq 1.0$) hexagonal phases obtained after heat treatment at 750 °C for 8 h.

dx.doi.org/10.1021/ic5009472 | Inorg. Chem. 2014, 53, 10101−10111

of a- (or b-) lattice parameter as a function of substituent content. It has been observed in the studies on hexagonal rare-earth ABO_3 systems that inspite of the large ionic radii variation at B-site (e.g., $YInO_3$ and $YMnO_3$), there is not much variation in the a- (b-) cell parameters when the solid solutions are formed between them retaining the hexagonal structure.[15] Thus, as long as the consecutive nominal compositions retain the hexagonal structure, ab plane would show smaller variations as compared to *c*-axis. However, on closely observing the peak shift in C-type phases, it is observed that the 2θ values corresponding to C-type peaks are shifting to lower values implying that the lattice parameter of the C-type phase is increasing. This indicates that on increasing the Fe^{3+} content in the $YInO_3$ lattice, when the phase separation into hexagonal and C-type sets in, the C-type phase is continuously getting richer in In^{3+} and the hexagonal phase is becoming richer in Fe^{3+}. On careful observation, a systematic increase in average broadening of XRD peaks belonging to hexagonal phase with increase in Fe^{3+} content can also be observed.

At 900 °C (Figure 1c), it was observed that only $YInO_3$ remains C-type cubic. Up to 60 mol % Fe^{3+} substitution in $YInO_3$, single- phasic hexagonal modification was observed and beyond that a new minor perovskite (orthorhombic) phase appeared which increases with increase in Fe^{3+} content. Under these conditions pure yttrium orthoferrite, ($YFeO_3$) now exists as single phasic orthorhombic polymorph which is the stable and known polymorph for this compound under ambient conditions. The conversion of hexagonal to orthorhombic modification is apparently driven by the tendency of lower symmetric BO_5 (B:In, Fe) and YO_7 polyhedra to adopt a more regular co-ordination upon increasing the temperature. Thus, at 900 °C, the phase relation clearly consists of all the three phases i.e. C-type cubic ($YInO_3$), hexagonal ($YIn_{1-x}Fe_xO_3$ ($0.1 \leq x \leq 0.6$)), and orthorhombic ($YFeO_3$). Biphasicity consisting of orthorhombic and hexagonal phase fields was observed for $YIn_{1-x}Fe_xO_3$ ($0.7 \leq x \leq 0.9$). The three types of polymorphs in ABO_3 observed in the present study are depicted in Figure 3.

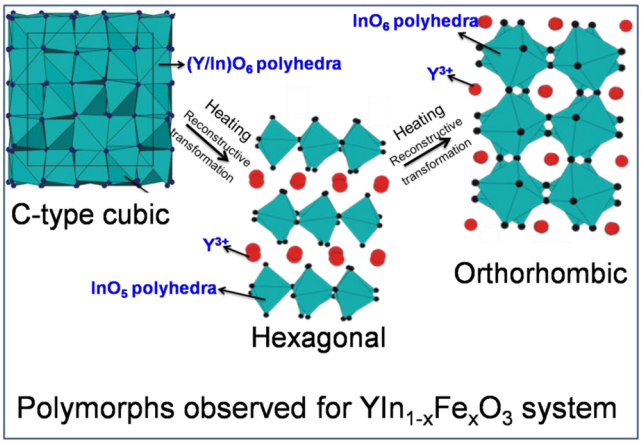

Figure 3. Schematic depiction of C-type, hexagonal, and orthorhombic phases observed.

Due to the dissimilarities in C-type, hexagonal and orthorhombic modifications, these are related to each other by reconstructive mode of phase transitions and are observed in the present system on subsequent heat- treatments.

Analyzing the phase relation at 1150 °C (Figure 1d) reveals that further heating has resulted in the extension of the biphasic regime and now the biphasic phase field consisting of orthorhombic and hexagonal polymorphs exists for nominal compositions $YIn_{1-x}Fe_xO_3$ ($0.5 \leq x \leq 0.9$). $YInO_3$ finally transforms from metastable C-type to hexagonal polymorph at this temperature. Close observation of the shifts observed in XRD patterns of samples heated at 1150 °C shows that in the hexagonal phase field there is a general shift of peaks to higher angle (due to decrease in average B-site cationic radii), but in the biphasic regime the peak positions for both the phases become almost constant, the only change being the relative concentration of two phases. Heating the system to 1200 °C converts even the Fe^{3+}-containing composition to a biphasic mixture of orthorhombic and hexagonal phases and the single-phasic hexagonal behavior was observed in $YIn_{1-x}Fe_xO_3$ ($0.0 \leq x \leq 0.3$). All the nominal compositions were then sintered at 1250 °C and no further variation in the phase relations was observed in $YIn_{1-x}Fe_xO_3$ ($0.0 \leq x \leq 1.0$) system. All the hexagonal nominal compositions, $YIn_{1-x}Fe_xO_3$ ($0.0 \leq x \leq 0.3$), were subjected to rietveld refinements. These three nominal compositions were the only ones chosen for refinement studies because the single-phasic hexagonal phases are the subjects of interest for electrical studies in the present work. The refined parameters are listed in Table 1 and the representative refined XRD patterns for nominal compositions $YInO_3$ and $YIn_{0.70}Fe_{0.30}O_3$ are shown in Figure 4. As is observed the lattice parameters decrease on increasing the Fe^{3+} content.

Figure 5 (bar diagram) summarizes the phase fields observed in the present system as a function of temperature. A close observation of the phase relations symbolized in Figure 5 clearly brings out few important results worth discussing.

(a) The existence of all the nominal compositions in C-type modification ($Ia\bar{3}$) is clearly an interesting result. Generally for ABO_3-type configuration, in order to predict the structure favored for a given pair of cations, a more complex radius relationship that includes structure-specific geometric arguments is utilized. The Goldschmidt's tolerance factor (defined in Introduction; given by $(r_A + r_O)/\sqrt{2}(r_B + r_O)$ is one such relationship.[5] Figure 5 lists the tolerance factors for all the nominal compositions studied in the $YIn_{1-x}Fe_xO_3$ ($0.0 \leq x \leq 1.0$) system. According to tolerance factors calculated for these nominal compositions,[5] $YInO_3$ should exist as stable hexagonal polymorph whereas orthorhombic structure should be the stable one known for $YFeO_3$. It is clear from the tolerance factor values of these nominal compositions [Figure 5] that all of them are well above the radius ratios required for crystallizing in C-type configuration. Because of the inherent nature of the C-type structure, the two cations should not have very different ionic radii in order to form a long-range disordered C-type structure, which is reflected in the lower tolerance factor for C-type structure.[5] Observation of C-type structure for $YFeO_3$ and other Fe-rich compositions is all the more intriguing because the ionic radii of Fe^{3+} (0.58 Å) is much smaller than Y^{3+} (0.90 Å) (reported in 6-fold co-ordination for C-type structure), for both of them to occupy sites with similar co-ordination number and crystallize as a long-range single-phasic C-type disordered structure. In fact, it has been stated by Pistorius et al.[32] that the C-type $YInO_3$ structure is obtainable at high temperature which is due to the randomization of dissimilar Y^{3+} and In^{3+} possible at higher temperature. Amrani et al. reported the synthesis of pure C-type structure of $YInO_3$ at 1400 °C.[33] This indeed makes the phase relation at 600 °C very interesting and unusual. The stabilization of the metastable C-type under these conditions could be due to kinetic

dx.doi.org/10.1021/ic5009472 | *Inorg. Chem.* 2014, 53, 10101−10111

Table 1. Rietveld Refined Parameters for $YIn_{1-x}Fe_xO_3$ (x = 0.0, 0.1, 0.2, and 0.3) after Heat Treatment at 1250 °C for 8 h

molecular formula	$YInO_3$	$YIn_{0.9}Fe_{0.1}O_3$	$YIn_{0.8}Fe_{0.2}O_3$	$YIn_{0.7}Fe_{0.3}O_3$
molecular weight	251.72	245.83	240.45	234.03
tolerance factor	0.8295	0.8350	0.8406	0.8463
space group	$P6_3cm$	$P6_3cm$	$P6_3cm$	$P6_3cm$
unit cell parameter				
a (Å)	6.2727 (1)	6.2512 (1)	6.2324 (1)	6.2080 (2)
b (Å)	6.2727 (1)	6.2512(1)	6.2324 (1)	6.2080 (2)
c (Å)	12.2563 (0)	12.1971(3)	12.1513 (3)	12.0917 (4)
vol (Å^3)	417.63 (9)	412.78 (1)	408.76 (2)	403.58 (2)
no. of parameters	10	10	10	10
refinement	Rietveld refinements (Fullprof-2K) (Rodriguez-Caravjal, 2000)			
profile	pseudovoigt			
goodness-of-fit (χ^2)	1.73	1.42	1.60	1.53
R_p	10.6	14.1	15.0	15.5
R_{wp}	15.3	19.8	20.5	21.2
R_F	5.56	6.67	7.5	8.26

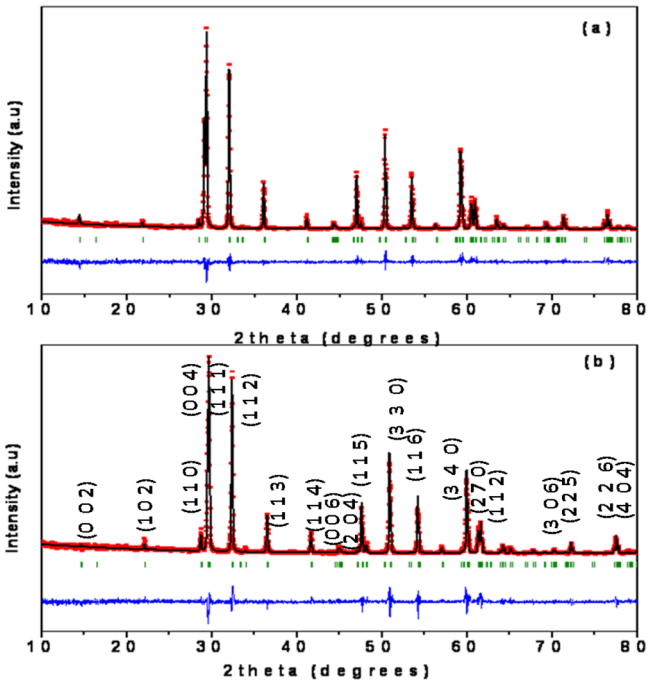

Figure 4. Typical fitted patterns of $YIn_{1-x}Fe_xO_3$ compositions (a) x = 0.0 and (b) 0.3 after heat treatment at 1250 °C for 8 h.

stabilization, which can be attributed to the non-equilibrium method of synthesis and the nanocrystalline nature of the product. The size difference between the A-site (Y^{3+}) and B-site ($In_{1-x}Fe_x$), decreases as In-content increases, making the relative ionic radii to move closer as required for C-type structures. This is plausibly the reason for much enhanced broadening of C-type peaks as the Fe-content increases, because accommodating Fe and Y in the same lattice at similar sites would produce much greater strain in the lattice. Precisely, because of the same reason, the compositions consisting of a higher amount of Fe tend to show phase transitions from C-type modification to hexagonal modifications at lower temperatures as compared to In-rich compositions. The higher the Fe-content, the higher the strain and hence the greater the tendency to transform to a stable modification.

(b) Further, the observation of hexagonal phase for $YIn_{1-x}Fe_xO_3$ ($0.3 \leq x \leq 0.9$) and even for $YFeO_3$ at 750 °C is also worth mentioning. This is again similar to discussion on C-type phase, because the presence of Fe^{3+} at the B-site is known to stabilize the orthorhombic modification in $REFeO_3$ (RE: rare-earth ions)! However, the fact that the broadening of XRD peaks increased on increasing Fe^{3+}-content showed that the strain in the lattice increases because hexagonal modification is obviously not the most stable arrangement with Fe at B-site.

(c) Surprisingly one particular nominal composition, $YIn_{0.1}Fe_{0.9}O_3$ has been found to exist in all the three polymorphs observed in this study, i.e., C-type, hexagonal and almost single-phasic orthorhombic as a function of temperature (though the orthorhombic phase exists with small impurity peaks belonging to hexagonal phase). This emphasizes that the synthesis route adopted has a strong bearing on the crystal chemistry, in particular when there are cations capable of adopting competing coordination polyhedra.

(d) The $YInO_3$-type hexagonal lattice has much higher solubility of Fe^{3+} as compared to In^{3+} into $YFeO_3$. This is supported by the fact that at 1150 °C 30 mol % of Fe^{3+} could be substituted in $YInO_3$ retaining the hexagonal modification. However, a biphasic region is observed even at 10 mol % In^{3+} substitution in orthorhombic $YFeO_3$. This is surprising considering the fact that In^{3+} is known to exist in 6-fold co-ordination (the B-site co-ordination in orthorhombic polymorph) in many ABO_3-type compounds. Obviously, the radius ratio of Y^{3+} and In^{3+} do not favor an orthorhombic crystalline arrangement.

3.2. Raman Spectroscopic Studies. It is widely known that vibrational techniques like IR and Raman spectroscopy can give information about subtle local variations in structures as difficult to reveal using diffraction techniques. Hence, the vibrational techniques can be used in tandem with diffraction techniques to study the "not very evident" local structural features, which often lead to remarkable functional properties.

There are not many reports on the Raman studies of hexagonal rare-earth indates. However, rare-earth hexagonal manganites, which have similar structure (sp. group $P6_3cm$), and are well-known multiferroic systems have been very well studied by Raman spectroscopy. In this work, the electrical studies were performed only on the monophasic compositions which showed hexagonal structure at 1250 °C, i.e., the nominal compositions $YIn_{1-x}Fe_xO_3$ ($0.0 \leq x \leq 0.3$). Hence in order to understand the subtle structural changes, Raman spectra were

dx.doi.org/10.1021/ic5009472 | Inorg. Chem. 2014, 53, 10101−10111

Fe^{3+} increasing

x* → / Temp ↓	$YInO_3$ x = 0	x = 0.1	x = 0.2	x = 0.3	x = 0.4	x = 0.5	x = 0.6	x = 0.7	x = 0.8	x = 0.9	$YFeO_3$ x = 1.0
(t)	0.8295	0.8350	0.8406	0.8463	0.8520	0.8579	0.8638	0.8698	0.8759	0.8820	0.8883
600 °C	C	C	C	C	C	C	C	C	C	C	C
750 °C	C	C	C + Hexa	Hexa	Hexa	Hexa	Hexa	Hexa	Hexa	Hexa	Hexa + Ortho
900 °C	C	Hexa	Hexa	Hexa	Hexa	Hexa	Hexa	Hexa + Ortho	Hexa + Ortho	Hexa + Ortho	Ortho
1150°C	Hexa	Hexa	Hexa	Hexa	Hexa	Hexa + Ortho	Hexa + Ortho	Hexa + Ortho	Hexa + Ortho	Hexa + Ortho	Ortho
1250°C	Hexa	Hexa	Hexa	Hexa	Hexa + Ortho	Hexa + Ortho	Hexa + Ortho	Hexa + Ortho	Hexa + Ortho	Hexa + Ortho	Ortho

Single phasic

Figure 5. Phase evolution in $YIn_{1-x}Fe_xO_3$ ($0.0 \leq x \leq 1.0$) system with temperature (C: C-type cubic ($Ia\bar{3}$) Hexa: Hexagonal perovskite related structure ($P6_3cm$) Ortho: orthrhombic perovskite structure ($Pnma$) t = tolerance factor).

recorded on all these nominal compositions which are shown in Figure 6.

The group theoretical analysis predicts a total of 60 phonon modes (10A1 + 5A2 + 10B1 + 5B2 + 15E1 + 15E2),[34] and only 38 of them, given by 9A1 + 14E1 + 15E2, are Raman active. In the present study, the major Raman bands for $YInO_3$ are observed at 152, 207, 217, 226, 246, 297, 323, 362, 376, 431, 508, 520, and 609 cm^{-1}. This is in agreement with that reported for $YMnO_3$ by Iliev et al.[34] in their Raman spectroscopic studies on $YMnO_3$. One major difference between the Raman spectra of $YInO_3$ and $YMnO_3$ is the shift in the corresponding wavenumbers. As is mentioned in our earlier report[28] on the $Y_{1-x}Gd_xInO_3$ system also, the Raman modes involving apical oxygens (609, 238 cm^{-1}, etc.) of BO_5 polyhedra are red-shifted in $YInO_3$ relative to $YMnO_3$ while modes involving planar oxygens (433 cm^{-1}, 297 cm^{-1}, etc.) do not vary much. The red shift can be attributed to relatively longer In−O apical bonds as compared to Mn−O bonds in $YMnO_3$. The insignificant variation in the modes involving planar oxygens can be attributed to the fact that in hexagonal $YMnO_3$ and $YInO_3$ the planar bond lengths do not differ much as is also shown by Smith et al.[15] for in $Y(In,Mn)O_3$ series.

A careful analysis of the Raman spectra reported for different nominal compositions in $YIn_{1-x}Fe_xO_3$ ($0.0 \leq x \leq 0.3$) [Figure 6] reveal that the number of the peaks appearing in all these is almost same indicating similar structures for them. However, there is a general broadening in the Raman bands. In fact in the Raman spectrum of $YIn_{0.7}Fe_{0.3}O_3$, several low frequency weak bands are not even observable due to the appreciable broadening. This can of course be attributed to the cation heterogeneity in the lattice due to partial substitution of In^{3+} by Fe^{3+}. With change in nominal composition, the relative composition at the B-site changes and the fact that In−O and Fe−O bonds will have different strengths will influence their vibrational frequencies resulting in the spread in frequency, and hence broadening of Raman modes is observed. There have been similar examples[35] wherein the substitution leads to the broadening of the Raman bands. A striking feature of the Raman spectra observed for indates is the relatively

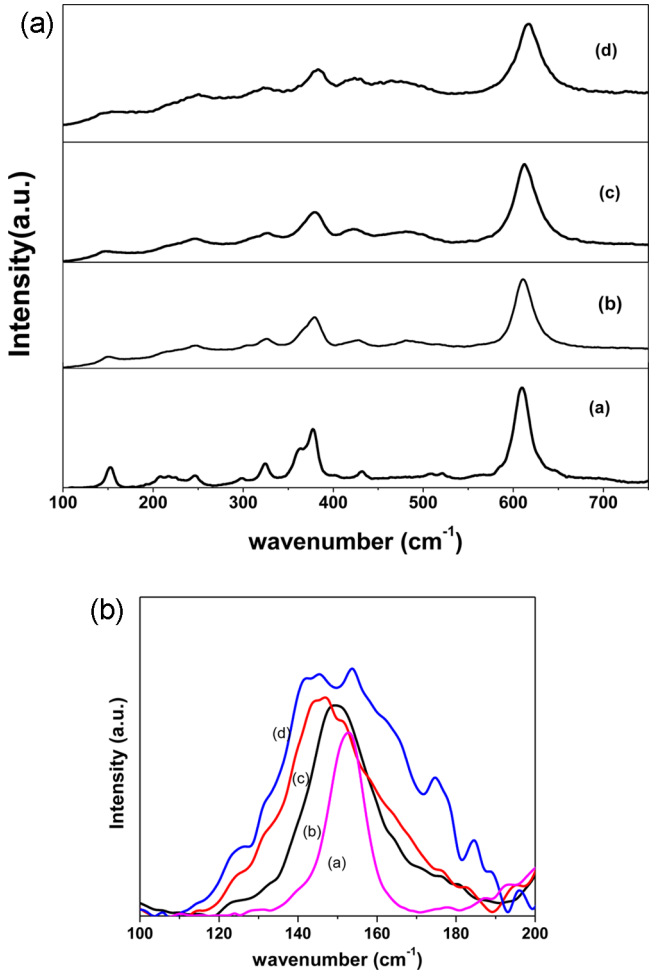

Figure 6. (a) Raman spectra of hexagonal $YIn_{1-x}Fe_xO_3$ with (a) x = 0.0, (b) 0.1, (c) 0.2, and (d) 0.3 after heat treatment at 1250 °C for 8 h. (b) Trend in wavenumber of Raman modes at 150 cm^{-1} for $YIn_{1-x}Fe_xO_3$ where x is (a) 0.0, (b) 0.1, (c) 0.2, and (d) 0.3.

dx.doi.org/10.1021/ic5009472 | Inorg. Chem. 2014, 53, 10101−10111

higher intensities of the 377 and 612 cm^{-1} bands, belonging to A_1 and E_1 symmetries, compared to other bands of same symmetry. It was also observed for the $Gd_{1-x}Y_xInO_3$ system.[28] The same has been observed by Iliev et al.[34] for $YMnO_3$, and this has been ascribed to the fact that each phonon mode of the non-centrosymmetric $P6_3cm$ space group has a zone boundary counterpart mode involving similar atomic motions in $P6_3/mmc$ space group. Due to relatively smaller distortion involved in bringing about the transition $P6_3cm$ to $P6_3/mmc$, A_1 and E_1 modes which correspond to the Raman-active A_{1g} and E_{1g} modes in $P6_3/mmc$ give much stronger bands compared to the Raman-inactive modes in $P6_3cm$. Both these bands show blue shift, i.e., shift to higher wavenumbers due to decrease in cell volume.

It is generally observed that the Raman frequencies depend largely on unit cell volume. It has been discussed in the previous section (XRD) that, on substituting Fe^{3+} for In^{3+} in $YInO_3$, the cell parameters as well as volume decreases which should lead to a general blue shift in the Raman modes. The decrease in lattice parameters (cell volumes) imply shortening of average bond length which indicates an increase in the force constant and hence increase in corresponding vibrational frequency or wavenumber which manifests as blue shift in the Raman modes. The shift in two of the representative Raman modes is depicted in Figure 7 and discussed herein. It is surprising to observe that while most of the modes show blue shift, some modes also show red shifts in their frequency values. One of the major modes at 608 cm^{-1} shows blue shift [Figure 7(a)]. This mode is related to apical B−O atom stretching vibration. The B atom in this case is In which is continuously getting substituted by Fe. Since the average size of the B-cation is decreasing, this implies decreasing B−O bond length which reflects in the blue shift of this mode. The most interesting feature of the Raman studies on this system is the red shift in the mode at 150 cm^{-1}[Figure 6b and7b]. In analogy with $YMnO_3$,[34,36−38] this mode corresponds to the Y displacement along the *c*-axis. Any change in this mode can be correlated to the change in Y−O distance. Thus, this suggests that the Y−O bond distance is elongating. The similar observations have also been made by other groups.[39,40] Adem et al.[39] studied the $YMn_{1-x}Ga_xO_3$ system by XRD and have stated that substitution at B-site leads to the elongation of YO_7 capped-antiprism along the *c*-direction. In their study, they have proposed that B-site substitution by a smaller ion leads to a greater change in Y−O (A-O) polyhedra rather than B−O polyhedra itself. A similar kind of elongation in Y−O polyhedra is suggested in the present study by the red shift in Y−O Raman mode (Figure 6b. This observation brings out the utility of vibrational techniques in detecting such subtle local changes for which diffraction techniques need more sophisticated sources.

3.3. Electrical Property Studies. In view of the interesting electrical properties exhibited by hexagonal $YMnO_3$ compounds[13] the main motivation of the present study was to carefully control the structure of the solid solutions in the $YIn_{1-x}Fe_xO_3$ system to tailor the electrical behavior. Hence, the nominal compositions exhibiting a single-phasic hexagonal structure at 1250 °C, i.e., the compositions $YIn_{1-x}Fe_xO_3$ ($0.0 \leq x \leq 0.3$) were subjected to the extensive dielectric studies. The variation of the dielectric constant (dielectric permittivity), ε' with temperature at several frequencies is shown in Figure 8 for the samples with x = 0.0, 0.1, 0.2, and 0.3. A remarkably composition dependent trend was revealed in the electrical behavior of these compositions. The dielectric constant at 30

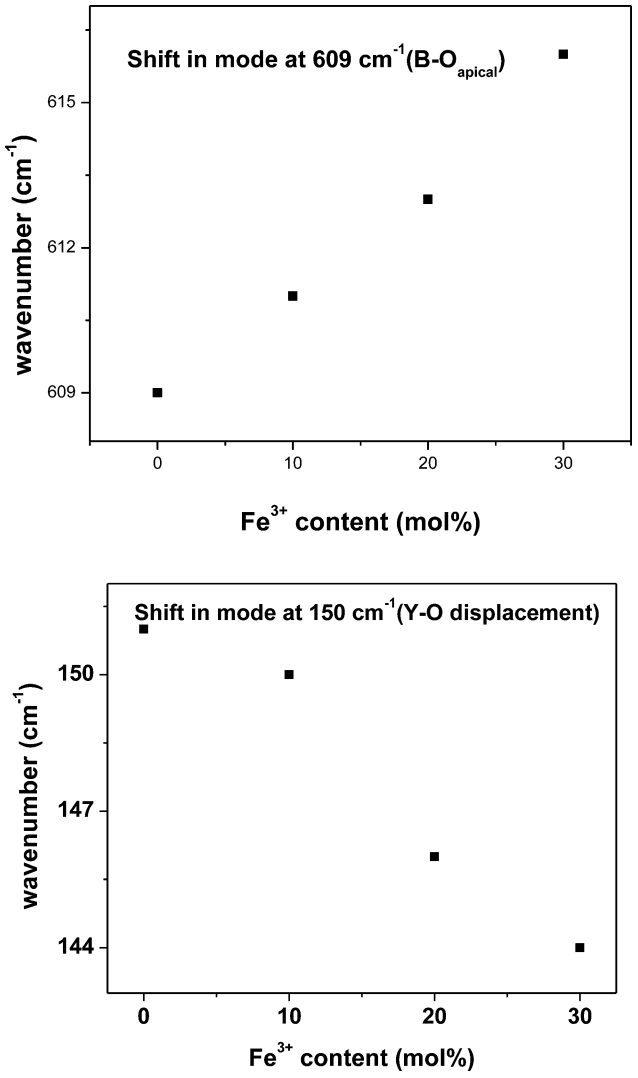

Figure 7. Shift in wavenumbers of two representative Raman modes.

°C and 100 Hz was found to increase from about 12 for x = 0.0 to as high as 1000 for x = 0.3, thus indicating the tremendous effect of addition of Fe in $YInO_3$ on the dielectric constant. This increase in the dielectric constant ε', indicates a plausible increase in the polarization (separation of charges), possibly due to formation of small dipolar regions when Fe is incorporated into the lattice.

A further interesting result was obtained by studying the temperature dependence of the dielectric constant of these nominal compositions and their variation with Fe content [Figure 8]. For pure $YInO_3$, ε' is almost constant as temperature rises, and then suddenly increases (near T = 175 °C at 100 Hz) and continues to increase with temperature, possibly due to the electronic conductivity and electrode polarization effects, especially at lower frequencies. It must be mentioned that $YInO_3$ is reported to be an improper ferroelectric with $T_c \approx 560$ °C.[41] However, in the present study, the temperature dependence of the electrical behavior has been studied only up to 300 °C, which could be the reason for non-observance of a peak in ε' vs T plot for parent $YInO_3$. For x = 0.1, i.e., for $YIn_{0.9}Fe_{0.1}O_3$, ε' shows a small step-like feature at about 75 °C (for 100 Hz), which has a significant frequency dependence. It further continues to increase steadily at temperatures beyond about 200 °C. There is also some

dx.doi.org/10.1021/ic5009472 | Inorg. Chem. 2014, 53, 10101−10111

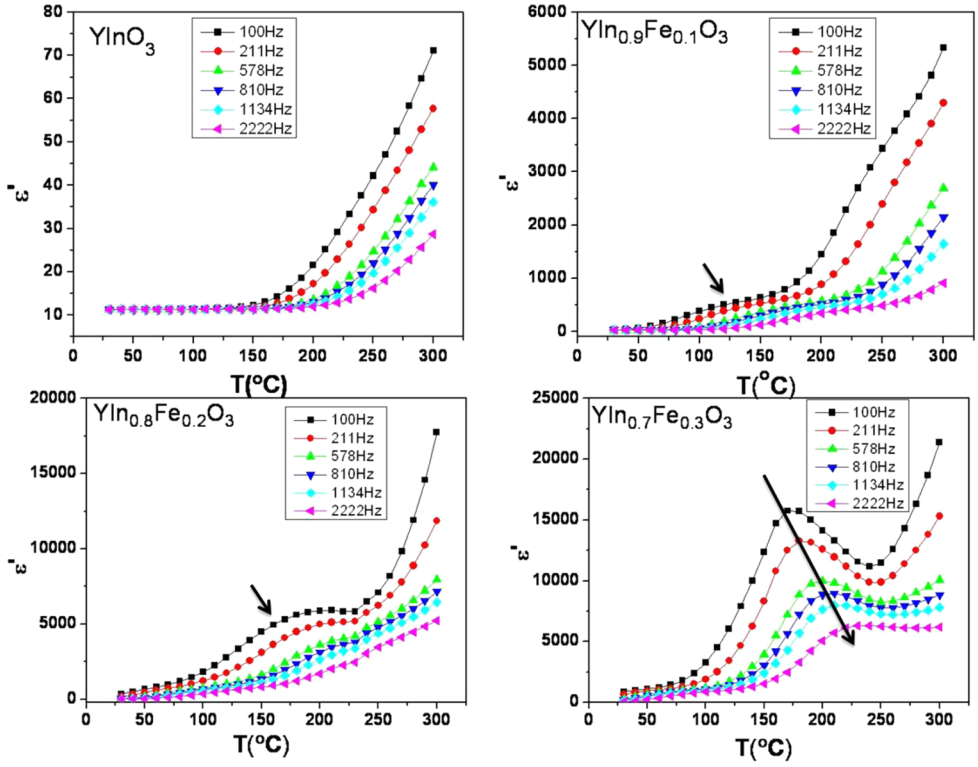

Figure 8. Dielectric constant vs temperature for hexagonal $YIn_{1-x}Fe_xO_3$ with x = 0.0, 0.1, 0.2, and 0.3.

evidence of a second dielectric relaxation beyond 200 °C. For the nominal composition $YIn_{0.8}Fe_{0.2}O_3$, the step-like feature is replaced by the appearance of a weak and broad peak, at lower frequencies near about 175 °C, with significant frequency dispersion. Most interestingly, for $YIn_{0.7}Fe_{0.3}O_3$, the dielectric constant at 100 Hz shows a broad peak near 175 °C with strong frequency dependence of the peak position, similar to that observed in relaxor ferroelectrics. The temperature dependence of the frequency of this dielectric relaxation was analyzed, and it was observed to show a Vogel–Fulcher-type behavior of the following form:

$$f = f_0 \exp(-E/k_B(T_m - T_{VF}) \quad (1)$$

where f_0 is a prefactor, k_B is the Boltzmann constant, T_m is the temperature of maximum permittivity, T_{VF} is the Vogel–Fulcher temperature, and E is the activation energy. The result of fitting eq 1 to the frequency–temperature behavior is shown in Figure 9. The best-fit values obtained were $f_0 = 1.5 \times 10^6$Hz, E = 0.09 eV, and T_{VF} = 344 K. This suggests a relaxor-like behavior for the x = 0.3 composition. The Vogel–Fulcher (V–F) behavior is usually associated with the freezing of dynamics, as in a liquid freezing to a glassy state upon cooling, or in spin glasses and the temperature T_{VF} is then interpreted as the temperature where all relaxations freeze. In relaxor ferroelectrics, it has been found that the V–F behavior always holds for the relaxation frequency. This is taken as an indication of freezing of the dynamics of polar nanoregions (PNR) that exist in these materials. However, it is now generally believed that the V–F behavior could also occur due to the gradual broadening of the relaxation time distribution and the broad maximum in permittivity, which are both characteristic features of relaxor ferroelectrics.[42] Figure 10 depicts the variation of reciprocal of dielectric constant with temperature. A deviation from ideal Curie–Weiss law is observed through the deviation

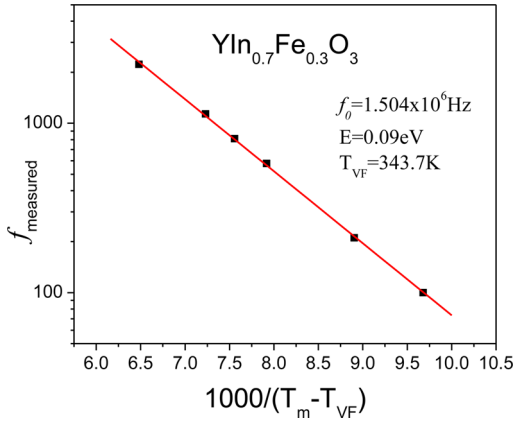

Figure 9. Vogel–Fulcher fit for the nominal composition $YIn_{0.7}Fe_{0.3}O_3$.

from straight line behavior in this plot. Such behavior is similar to that exhibited by relaxor ferroelectrics.

The dielectric loss (tan δ) vs temperature is plotted for various nominal compositions, $YIn_{1-x}Fe_xO_3$ ($0.0 \leq x \leq 0.3$), and depicted in Figure 11. It is observed that the dielectric loss factor at room temperature and 100 Hz takes values of 0.003 (very low loss) for $YInO_3$. However, it increases to 1.2 for x = 0.1, and then decreases to 0.6 for x = 0.3. Interestingly, evidence for two dielectric relaxation processes can be seen for all the compositions studied except undoped $YInO_3$. Also, it was observed that the magnitude of the low frequency relaxation is almost the same, while that of the high temperature relaxation increases with increasing x. The high temperature relaxation may be related to the relaxor-like behavior while the lower temperature relaxation may be due to hopping of charge-carriers although the origin is not clear.

dx.doi.org/10.1021/ic5009472 | Inorg. Chem. 2014, 53, 10101–10111

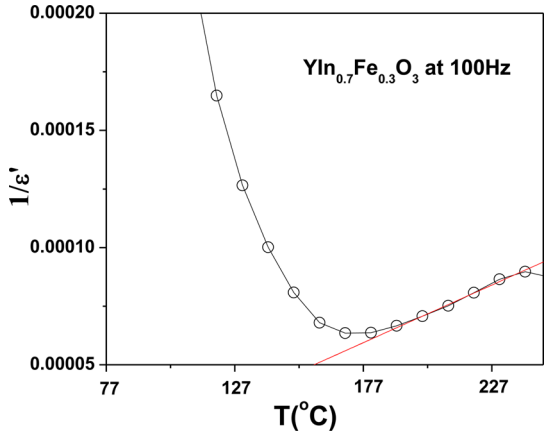

Figure 10. Plot of reciprocal of dielectric constant vs temperature (at 100 Hz).

All three observations, i.e., (a) strong frequency dispersion of the peak of the dielectric constant with temperature plots, (b) Vogel–Fulcher type behavior of dielectric relaxations, and (c) deviation from ideal Curie–Weiss behavior, strongly suggest the ferroelectric relaxor like dynamics for $YIn_{0.7}Fe_{0.3}O_3$ nominal composition. The dielectric studies on this $YIn_{1-x}Fe_xO_3$ ($0.0 \leq x \leq 0.3$) system in the temperature range of 25 to 300 °C suggest that the electrical behavior of the given system could be gradually tuned from a normal dielectric to ferroelectric relaxor-like material.

The composition-induced relaxor behavior has been observed on substituting heteroatom in known ferroelectrics or incipient ferroelectrics. There have been many reports on $BaTiO_3$-based system regarding such relaxor behavior.[43] Such composition driven-relaxor behavior was also observed by Mani et al. in $FeTiTaO_6$.[44] However, to the best of our knowledge, there have been fewer studies on hexagonal ABO_3-type compounds wherein relaxor behavior has been studied as the function of dopant (substituent)-content. Some studies on heteroatom substitution have been performed by our group on $GdSc_{1-x}In_{1-x}O_3$ ($0.0 \leq x \leq 1.0$)[22] and $Gd_{1-x}Y_xInO_3$ ($0.0 \leq x \leq 1.0$)[23] wherein substitutions were done at B and A sites, respectively.

From the comparison of earlier two studies,[27,28] it was deduced that variation of electrical behavior is more influenced by tempering the B-site. The present study further reiterates this observation. These hexagonal rare-earth indates (or manganites) owe their ferroelectric properties to the spontaneous polarization bestowed upon them due to structural features. It has been reported that these structures consist of InO_5 trigonal bipyramids (TBP) and YO_7 capped trigonal antiprisms and the ferroelectricity is induced due to unequal Y–O bond lengths along the *c*-axis. This is primarily governed by the buckling of InO_5 TBPs with respect to the *c*-axis or the vertical axis of YO_7 antiprisms. From the comparison of these three studies, it is apparent that substitution at B-site (here Fe for In), distorts BO_5 polyhedra and this in turn subtly alters YO_7 antiprism. If the schematic diagram of BO_5 and AO_7 polyhedra in hexagonal ABO_3 is carefully observed [Figure 12], it is evident that any distortion in BO_5 polyhedra will affect AO_7

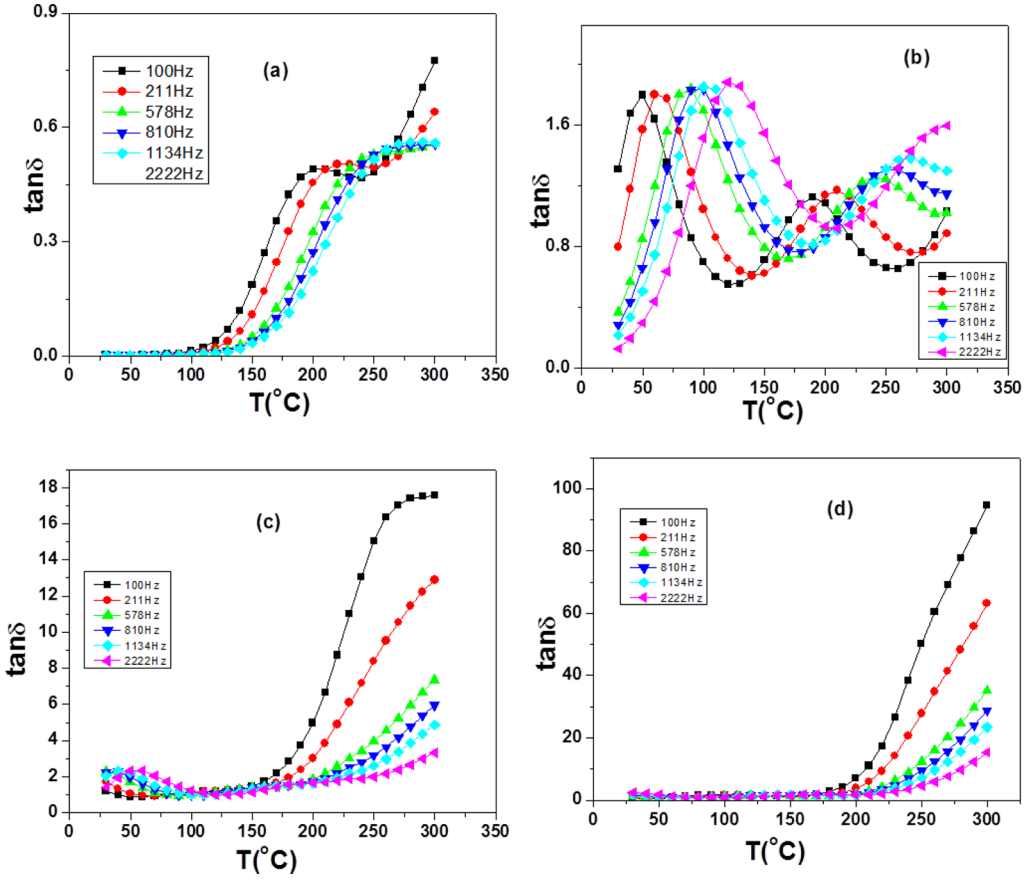

Figure 11. Dielectric loss vs temperature for hexagonal $YIn_{1-x}Fe_xO_3$ (a) $x = 0.0$, (b) 0.1, (c) 0.2, and (d) 0.3.

dx.doi.org/10.1021/ic5009472 | Inorg. Chem. 2014, 53, 10101–10111

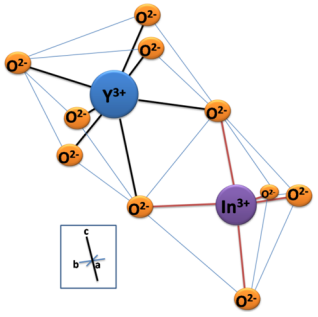

Figure 12. Schematics of polyhedral connection of YO_7 and (In/Fe)O_5 polyhedra in $YIn_{1-x}Fe_xO_3$.

bond lengths, thereby disturbing the original ferroelectric arrangement and introducing relaxor behavior. It is obvious that an increasing amount of Fe^{3+} is progressively increasing distortion in BO_5 polyhedra which apparently leads to variations in Y−O bond lengths. This is instrumental in controlling the electrical behavior of hexagonal indates. This is also supported by the red shift in the Raman band at frequency 150 cm^{-1} which pertains to Y−O−Y motion (as discussed in previous section) when all other Raman bands show blue shift. Whereas on the other hand, it appears that substitution at the A-site in $YInO_3$[28] simply randomizes the A-site without much effect on relative arrangement of atoms which controls geometric ferroelectricity.

4. CONCLUSIONS

The $YIn_{1-x}Fe_xO_3$ $(0.0 \leq x \leq 1.0)$ mixed oxides were synthesized and explored for structural behavior and electrical properties. The phase relations showed very rich crystal chemistry, and a variety of phases like metastable C-type, hexagonal, and orthorhombic modifications were observed as a function of temperature and composition. An unexpected red shift in the mode belonging to Y−O displacement providing the direct evidence of effect of B-site substitution on YO_7 polyhedra was observed by Raman spectroscopy. A highlight of the study is the introduction of relaxor behavior in hexagonal $YInO_3$ on substituting Fe^{3+} which ultimately led to a classical ferroelectric relaxor like behavior in $YIn_{0.7}Fe_{0.3}O_3$ nominal composition. The compositional control and the distortion brought about in (In/Fe)O_5 polyhedra have been invoked to explain this behavior. The study stresses the importance of subtle local structural changes affecting the bulk electrical behavior and brings out the significance of controlling the composition and the structure to tune electrical properties.

AUTHOR INFORMATION

Corresponding Authors

*Phone: 0091-22-2559 5330. Fax: 0091-22-25505151. E-mail: vinita@barc.gov.in.

*E-mail: aktyagi@barc.gov.in.

Notes

The authors declare no competing financial interest.

ACKNOWLEDGMENTS

The Department of Atomic Energy's Science Research Council (DAE-SRC) is acknowledged for supporting this work vides sanction number no. 2010/21/9-BRNS/2025 dated 7-12-2010. Dr. V. K. Jain, Head, Chemistry Division, BARC, is thanked for his keen interest.

REFERENCES

(1) Bedekar, V.; Shukla, R.; Tyagi, A. K. *Nanotechnology* **2007**, *18*, 155706.
(2) Brik, M. G.; Srivastava, A. M. *ECS J. Solid State Sci. Technol.* **2013**, *2*, R148−R152.
(3) Sullivan, E.; Vogt, T. *ECS J. Solid State Sci. Technol.* **2013**, *2*, R3088−R3099.
(4) Anderson, M. T.; Greenwood, K. B.; Taylor, G. A.; Poeppelmeier, K. R. *Prog. Solid. State Chem.* **1993**, *22*, 197−233.
(5) Giaquinta, D. M.; zur Loye, H.-C. *Chem. Mater.* **1994**, *6*, 365−372.
(6) Katsufuji, T.; Mori, S.; Masaki, M.; Moritomo, Y.; Yamamoto, N.; Takagi, H. *Phys. Rev. B* **2001**, *64*, 104419(1)−104419(6).
(7) Yakel, H.; Koehler, W.; Bertaut, E.; Forrat, F. *Acta Crystallogr.* **1963**, *16*, 957−962.
(8) Van Aken, B. B.; Meetsma, A.; Palstra, T. M. *Acta Crystallogr.* **2001**, *230*, c57.
(9) Ismailzade, I. G.; Kizhaev, S. A. *Sov. Phys. Solid State* **1965**, *7*, 236−238.
(10) Floros, N.; Rijssenbeek, J. T.; Martinson, A. B.; Poeppelmeier, K. R. *Solid State Sci.* **2002**, *4*, 1495−1498.
(11) Vander Griend, D. A.; Malo, S.; Wang, K. T.; Poeppelmeier, K. R. *J. Am. Chem. Soc.* **2000**, *122*, 7308−7311.
(12) Malo, S.; Maignan, A.; Marinl, S.; Hervieu, M.; Poeppelmeier, K. R.; Raveau, B. *Solid State Sci.* **2005**, *7*, 1492−1499.
(13) Van Aken, B. B.; Palstra, T. T. M.; Filippetti, A.; Spaldin, N. A. *Nat. Mater.* **2004**, *3*, 164−170.
(14) Zhang, Y.; Yang, J.; Xu, J.; Gao, Q.; Hong, Z. *Mater. Lett.* **2012**, *81*, 1−4.
(15) Smith, A. E.; Mizoguchi, H.; Delaney, K.; Spaldin, N. A.; Sleight, A. W.; Subramanian, M. A. *J. Am. Chem. Soc.* **2009**, *131*, 17084−17086.
(16) Tamilarasan, S.; Sarma, D.; Reddy, M. L. P.; Natarajan, S.; Gopalakrishnan, J. *RSC Adv.* **2013**, *3*, 3199−3202.
(17) Yakel, H. L.; Koehler, W. C.; Bertaut, E. F.; Forrat, E. F. *Acta Crystallogr.* **1963**, *16*, 957−962.
(18) Smolenskii, G. A.; Bokov, V. A. *J. Appl. Phys.* **1964**, *35*, 915−917.
(19) Lukaszewicz, K.; Karut-Kalicinska. *J. Ferroelectrics* **1974**, *7*, 81−82.
(20) Lottermoser, T.; Fiebig, M.; Fröhlich, D.; Kallenbach, S.; Maat, M. *Appl. Phys. B: Laser Opt.* **2002**, *74*, 759−764.
(21) Sleight, A. W. *Prog. Solid State Chem.* **2009**, *37*, 251−261.
(22) Shvartsman, V. V.; Lupascu, D. C. *J. Am. Ceram. Soc.* **2012**, *95*, 1−26.
(23) Bokov, A. A.; Ye, Z.−G. *J. Mater. Sci.* **2006**, *41*, 31−52.
(24) Kleemann, W. *Int. J. Mod. Phys. B* **1993**, *7*, 2469−507.
(25) Kirillov, V. V.; Isupov, V. A. *Ferroelectrics* **1973**, *5*, 3−9.
(26) Blinc, R.; Pirc, R. *Phys. Rev. B* **1999**, *60*, 13470−8.
(27) Grover, V.; Shukla, R.; Jain, D.; Deshpande, S. K.; Arya, A.; Pillai, C. G. S.; Tyagi, A. K. *Chem. Mater.* **2012**, *24*, 2186−2196.
(28) Shukla, R.; Grover, V.; Deshpande, S. K.; Jain, D.; Tyagi, A. K. *Inorg. Chem.* **2013**, *52*, 13179−13187.
(29) Tohei, T.; Moriwake, H.; Murata, H.; Kuwabara, A.; Hashimoto, R.; Yamamoto, T.; Tanaka, I. *Phys. Rev. B* **2009**, *79*, 144125.
(30) Purohit, R. D.; Sharma, B. P.; Pillai, K. T.; Tyagi, A. K. *Mater. Res. Bull.* **2001**, *36*, 2711−2721.
(31) Shannon, R. D. *Acta Crystallogr.* **1976**, *A32*, 751−767.
(32) Pistorius, C. W. F. T.; Kruger, G. J. *J. Inorg. Nucl. Chem.* **1976**, *38*, 1471−1475.
(33) Amrani, M. El.; Phuoc, V. Ta; Ammar, M. R.; Zaghrioui, M.; Gervais, F. *Solid State Sci.* **2012**, *14*, 1315−1320.
(34) Iliev, M. N.; Lee, H. G.; Popov, V. N.; Abrashev, M. V.; Hamed, A.; Meng, R. L.; Chu, C. W. *Phys. Rev. B* **1997**, *56*, 2488−2494.
(35) Banerji, A.; Grover, V.; Sathe, V.; Deb, S. K.; Tyagi, A. K. *Solid State Commun.* **2009**, *149*, 1689−1692.
(36) Kim, J.; Jung, S.; Park, M.; Lee, S. I.; Cheong, H. D.; Kim, K. H.; Choi, E. J. *Phys. Rev. B* **2006**, *74*, 052406.
(37) Zaghrioui, M.; Phuoc, V. Ta; Souza, R. A.; Gervais, M. *Phys. Rev. B* **2008**, *78*, 184305.

(38) Fukumura, H.; Matsui, S.; Harima, H.; Kisoda, K.; Takahashi, T.; Yoshimura, T.; Fujimura, N. *J. Phys.: Condens. Matter* **2007**, *19*, 365239.
(39) Adem, U.; Nugroho, A. A.; Meetsma, A.; Palstra, T. T. M. *Phys. Rev. B* **2007**, *75*, 014108.
(40) Zaghrioui, M.; Phuoc, V. Ta. *Solid State Commun.* **2011**, *151*, 1704−1707.
(41) Abrahams, S. C. *Acta Crystallogr.* **2001**, *B57*, 485−490.
(42) Bokov, A. E.; Ye, Z.-G. *J. Adv. Diel.* **2012**, *2*, 1241010.
(43) Ferrarelli, M. C.; Tan, C. C.; Sinclair, D. C. *J. Mater. Chem.* **2011**, *21*, 6292−6299.
(44) Mani, R.; Achary, S. N.; Chakraborty, K. R.; Deshpande, S. K.; Joy, J. E.; Gopalakrishnan, J.; Tyagi, A. K. *Adv. Mater.* **2008**, *20*, 1348−1352.